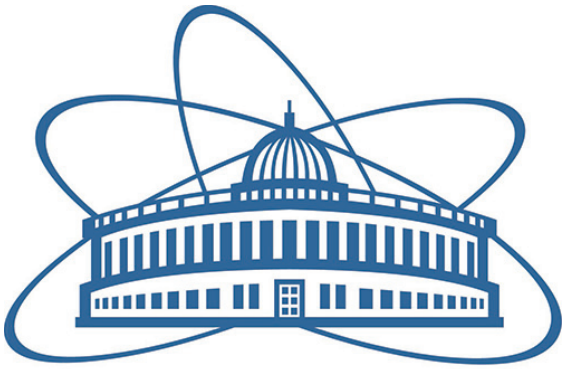

Joint Institute for Nuclear Research
Flerov Laboratory of Nuclear Reactions (FLNR)

Final Report on the INTEREST Programme

INTErnational REmote STudent Training Programme
(Wave 10, 26 February - 14 April, 2024)

Prompt gamma-ray spectroscopy using segmented High-Purity Germanium (HPGe) detectors

Supervisor

Dr. Aniruddha Dey

Student

Utkarsh Bajpai

Indian Institute of Science Education and Research (IISER)

Mohali, India

Dubna, 2024

Contents

Acknowledgements

I express my sincerest gratitude to Dr. Aniruddha Dey, for providing me with this wonderful opportunity to participate in an online research project at one of the best institutions in nuclear and high-energy physics. I am indebted for the numerous lectures, help sessions that he provided, without which I could not have imagined completing this project. I owe extreme gratitude to him for sharing the experimental spectra, literature as well helping me with the computational procedures ranging from the software installation to the plotting of the final results as well as taking time out of his tight schedule and providing valuable inputs for the weekly reports and analysis. I am very grateful for his accommodating and warm nature. The learning and experience gained in this project were tremendous and will be invaluable for my future prospects. I always look forward to working with him on future projects. I am sincerely thankful to my co-participant in this project, An Binh Le for his valuable contributions during the meetings and presentation on photoelectric absorbtion.

My special thanks to the JINR INTEREST team for granting me this opportunity and smoothly conducting the whole process and organizing a highly unique and innovative program.

Last but not the least, I would like to sincerely thank every individual who, in some way or another, contributed to this project.

Abstract

High resolution gamma spectroscopy is crucial for understanding the nuclear structure and dynamics. High purity germanium(HPGe) detectors offer excellent energy resolution and are ideal for these studies. We study the various γ interactions and simulation of Klein Nishina cross section has been carried out. The present work aims to understand the γ detector mechanisms with focus on the HPGe detectors. Ideality of germanium as a material for gamma detection has been established through a comparative analysis of attenuation coefficients. Energy calibration function has been obtained through linear and quadratic fitting of the analysed data from the clover crystals. Variation of the energy resolution and peak FWHM with the γ energy has been presented. Photopeak efficiency has been increased by applying the anti-compton BGO shield and the addback mode merging the spectra from the composite Clover detector. The counts in photopeak have been compared between addback and the sum mode. Potential of large arrays of composite HPGe in revolutionising the future of experimental nuclear physics studies has been realised.

Chapter 1

Introduction to gamma-ray spectroscopy

1.1 Motivation

High resolution gamma spectroscopy is the key to understanding the nuclei structure, reaction dynamics as well as in quite a few societal applications. The high resolution greatly facilitates measurement of nuclear properties of nuclei decaying through complex-level schemes by disentangling the gamma rays from the background, *separating the needles from the haystack.* The high purity germanium (HPGe) detectors are indispensable for such experiments owing to their excellent energy resolution (0.2%) at 662 keV as compared to 6% for the commonly used NaI scintillator detector. However, the HPGe detector have relatively low efficiency due to small crystal size. The γ capture probability can be enhanced by employing arrays of these smaller HPGe detectors, such as the *Clover* and the *Cluster* comprising of 4 and 8 crystals respectively.

In this project, we highlight the need for HPGe detectors in high-resolution gamma spectroscopy. This will be followed by the characterization of individual germanium crystals of a Clover detector. The addback procedure has been applied to combine the individual spectra and compared with the direct summing of the spectra from the individual crystals.

1.2 Gamma Spectroscopy

The energy level spacing in atomic nuclei fall in the region of gamma radiation, from hundreds of keV to few MeV. The transitions connecting these levels are followed by emission of energy in form of γ rays. Spectroscopy can be understood as combination of spectrum(breaking of light) and scopy(looking into details). Gamma spectroscopy refers to looking into the gamma rays and extracting physical information about he atomic nuclei emitting them. The information can range from energy level, intensity, spin, parity, electromagnetic characters, lifetimes etc. These gamma rays uniquely characterize an atomic nuclei and are way of communicating with the atomic nuclei.

Since these γ rays are invisible to human eyes, we need special eyes in form of detectors to detect and measure these gamma-ray energies, timing etc. The various types of detectors are characterised in terms of the physical state of their detecting media such as solid (scintillator and semiconductors), gas detectors and liquid detectors. In upcoming chapters we discuss the advantage of using the germanium based semiconductor detector for gamma spectroscopy.

Chapter 2

Gamma-ray interaction mechanism

Understanding the interactions of γ rays with matter is key to correlate the γ spectrum features to the nuclear properties like shape, energy levels, lifetimes, moments etc.

The different interactions mechanisms manifests as different features in the γ spectrum as shown in Figure 2.1.

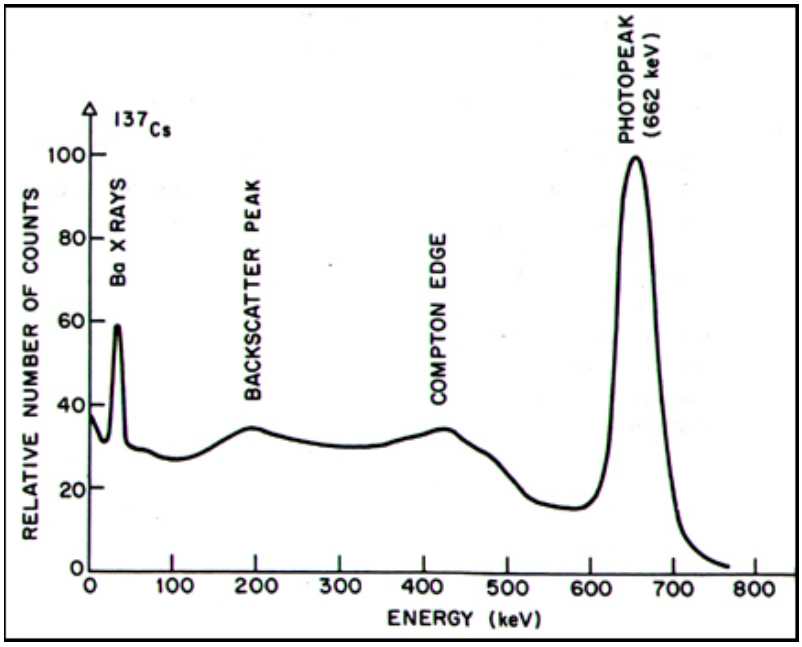

Figure 2.1: Gamma spectrum of ^{137}Cs

2.1 Gamma Interactions relevant for present analysis

2.1.1 Photoelectric Absorbtion

Photoelectric absorbtion is most important for nuclear structure as the photon deposits its entire energy inside a detector. Incoming photon is absorbed by a bound electron and transfers all its energy to the binding energy and kinetic energy of the ejected photo-electron. The photoelectric absorption increases with number of electrons in the detector material, varying as Z^n , n between 4 to 5.

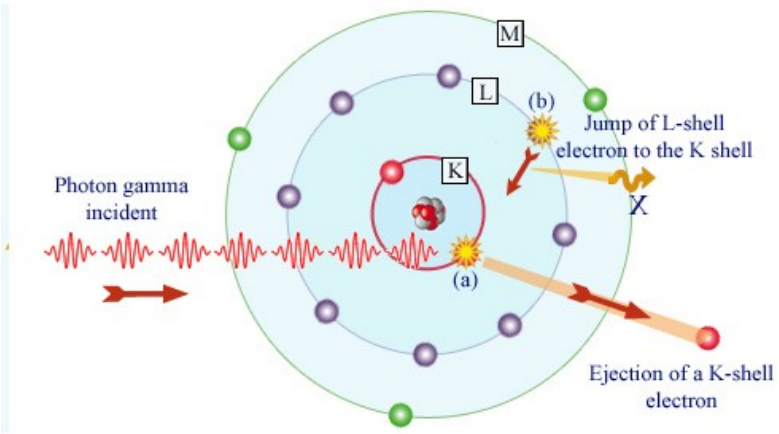

Figure 2.2: Photoelectric absorbtion

A photon can transfer all its energy only to a bound electron. Let us see the proof by contradiction.

$$\vec{p1} + \vec{p} = \vec{p2} \tag{2.1}$$

Squaring and substituting $p = p2 - p1$

$$(p2 - p1)\left[\sqrt{p1^2c^2 + m_e c^2} - p1c\right] = 0 \tag{2.2}$$

The possible solutions require

$$p1 = p2$$

This is the violation of linear momentum conservation Eq. 2.1

$$m_e = 0$$

This requires the electron to be massless, which is clearly not true. In other words, it means that the electron needs be travelling with velocity of light, c. This leads to violation of the principle of special relativity.

Thus, photoelectric effect which involves complete energy deposition by a γ can not occur with free electron. The bound electron can participate in the photoelectric effect as the the nucleus can recoil and aid in photon conservation. Further a part of energy of γ is spent in releasing the binding energy(BE) of the electron.

$$E_e = E_\gamma - BE \tag{2.3}$$

2.1.2 Compton Scattering

Incoming γ photon interacts with a nearly free electron, transferring only a fraction of its energy(E_γ) and deflects at an angle θ from initial trajectory. From momentum and energy conservation can calculate the energy of scattered gamma photon $E_{\gamma'}$

$$E_{\gamma'} = \frac{E_\gamma}{1 + \frac{E_\gamma}{m_0 c^2}(1 - \cos\theta)} \tag{2.4}$$

Figure 2.3 shows the modeled variation of the scattered photon energy with the scattering angle. This produces a continuous background lower energy of incident energy, corresponding to scattering angle. It is also characterized by a *Compton edge* correspond to maximum energy transfer at 180 degrees.

The energy of recoil electron is then given as

$$E_e = E_\gamma - E_{\gamma'} \tag{2.5}$$

The Compton interaction probability varies linearly with the number of electrons, ($\approx Z$) of the detector.

2.1.3 Pair Production

The electron-positron pair production is effective at $E_\gamma > 2m_0c^2 = 1.022$ MeV, that is the minimum energy (KE =0) for a e^-e^+ pair. A γ photon near Coloumb field of nucleus splits producing e^-e^+. Further the positron can annihilate with material

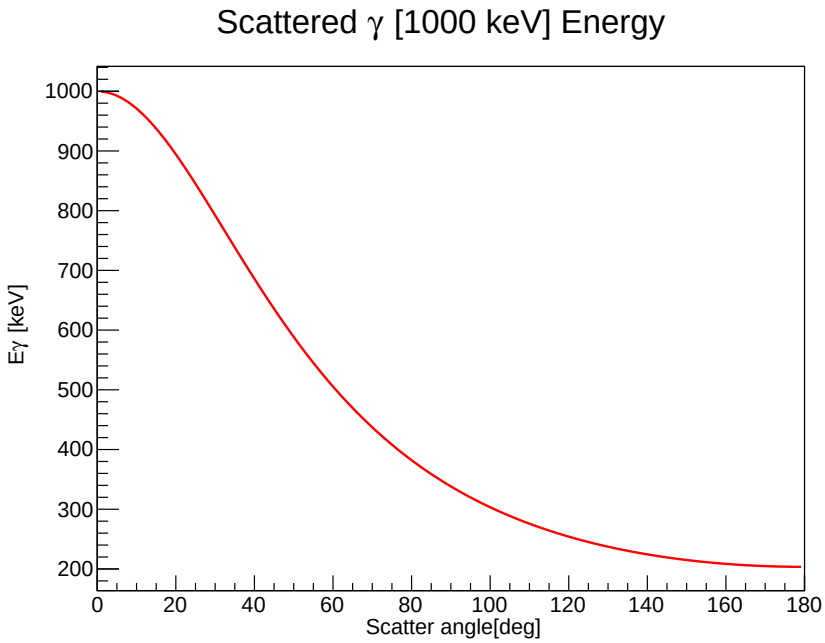

Figure 2.3: Scattered photon energy variation with the angle of scattering for an incident photon of 1 MeV

electrons to produce two γ of 511 keV each. One(Two) 511 keV γ can escape the detector producing a peak at $E_\gamma - 511(E_\gamma - 1022)$ keV.

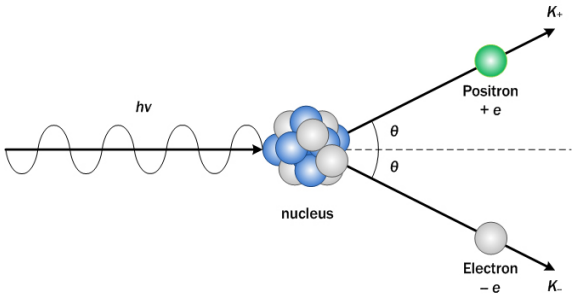

Figure 2.4: Pair Production

Pair production can only occur near a nucleus influenced by its Coulomb field. We will try to see the proof by considering a pair production in free space Figure 2.4. The angle θ will be same for e^- and $e+$ since the linear momentum is conserved in perpendicular direction. Conservation of energy implies $E_\gamma = E_e^- + E_e^+$

$$h\nu = 2\gamma m_0 c^2 \tag{2.6}$$

Conserving momentum in direction of photon gives

$$\frac{h\nu}{c} = 2\gamma m_0 v \cos\theta \tag{2.7}$$

Here, $m\vec{v} = m_0\gamma\vec{v}$ is the linear momentum of electron and positron each and $\gamma = \frac{1}{\sqrt{1-\frac{v^2}{c^2}}}$
Since $\frac{v}{c} < 1$ and $\cos\theta < 1$, Eq. 2.7 implies

$$h\nu < 2\gamma m_0 c^2 \tag{2.8}$$

Thus energy conservation Eq. 2.6 and linear momentum conservation Eq 2.6 contradict each other.

This means, pair production cannot occur in vacuum and requires present of other nucleus which can recoil and take some energy of the incident γ photon, thus conserving momentum and energy.

2.2 Other Interactions

2.2.1 Rayleigh Scattering

It is an elastic scattering, meaning there is no photon energy loss and the phase is unaltered. It occurs for photon energy less than 0.1 MeV in high Z materials.

2.2.2 Photo Disintegration

Photo disintegration of nucleus occurs when a nucleus absorbs a high-energy γ photon and immediately disintegrates into lighter elements. Often a neutron, proton or an alpha particle is released in this process. This is quite of importance in nuclear astrophysics reactions.

2.3 Attenuation Coefficients

The mass attenuation coefficient $\frac{\mu}{\rho}$ describes the change in intensity I for an incident beam of mono-energetic photons with intensity I_0 . Mathematically, the change in intensity suffered by a beam in passing a material of density ρ and mass thickness x, can be expressed as

$$\frac{I}{I_0} = \exp\{-(\mu/\rho)x\}$$

The mass thickness x is related to the thickness t as $x = \rho x$

Figure 2.5 shows the variation the mass attenuation coefficient with the photon energy. A comparison between different Z material is presented. The data is taken from the NIST database [7]. It is observed that the till 1 MeV, lead (Z = 82) has the highest mass attenuation coefficient. Thus, a indicent photon beam will suffer maximum intensity reduction through lead, making it a suitable shielding material. The energy to release a electron from a K shell, marked by the first peak is very less in germanium as compared to lead, this explains why *germanium is good detector and lead is a good shield.*

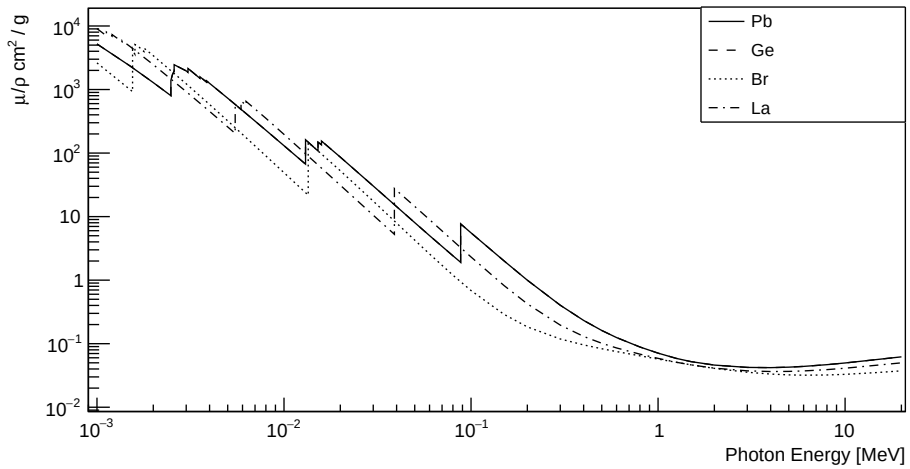

Figure 2.5: Differential cross sections for various photon interaction as a function of energy. Plotted using data from [7]

2.4 Interaction Cross Sections

The cross-section signify the probability of a reaction between an incident projectile and a target material or detector. The cross section is a function of the photon energy as well as the atomic number, Z of the target material. The relation between cross section, energy E and Z is usually based on semi-empirical studies, using experimental evidence to correct the prevalent model. The interaction processes for a photon and their cross-sections are summarized below

1. Photoelectric: At low energy $\sigma_{PE} \approx \frac{Z^4}{E^3}$ and at high energies $\sigma_{PE} \approx \frac{Z^5}{E}$

2. Incoherent (Compton) scattering The cross-section energy dependence is given by the Klein Nishina formula in the high energy limit. This is discussed in Section 2.5. The cross section varies linearly with Z, that is, the number of electrons or the scattering particles.

3. Pair Production The cross-section varies $\approx Z^2 \ln E$. The Z^2 term stems from the Coulomb field interaction of this process.

4. Coherent (Rayleigh/Thomson scattering): involves scattering of the photons by an atom as a whole. No energy transfer between the ephotons and electrons is involved. The incident photons are deviated at small angles. The cross section varies as $\approx \frac{Z}{E^2}$

5. Delbruck scattering: scattering of a photon by a electrostatic Coulomb field of the nucleus, it is also referred as *scattering of light by light*. The Z dependence goes as $\approx Z^4$. Being closely related to the process of pair production, it has aa similar dependence on the energy E, however the Delbruck scattering can take place at energies lower than the 1.022 MeV as well. [1]

6. Photonuclear reactions are significant for high energetic photons. The nucleus splits into nucleons following absorption of a photon. The cross sections for photonuclear reactions exhibit a broad peak at 23 MeV for low Z and at 12 MeV for high Z absorbers.

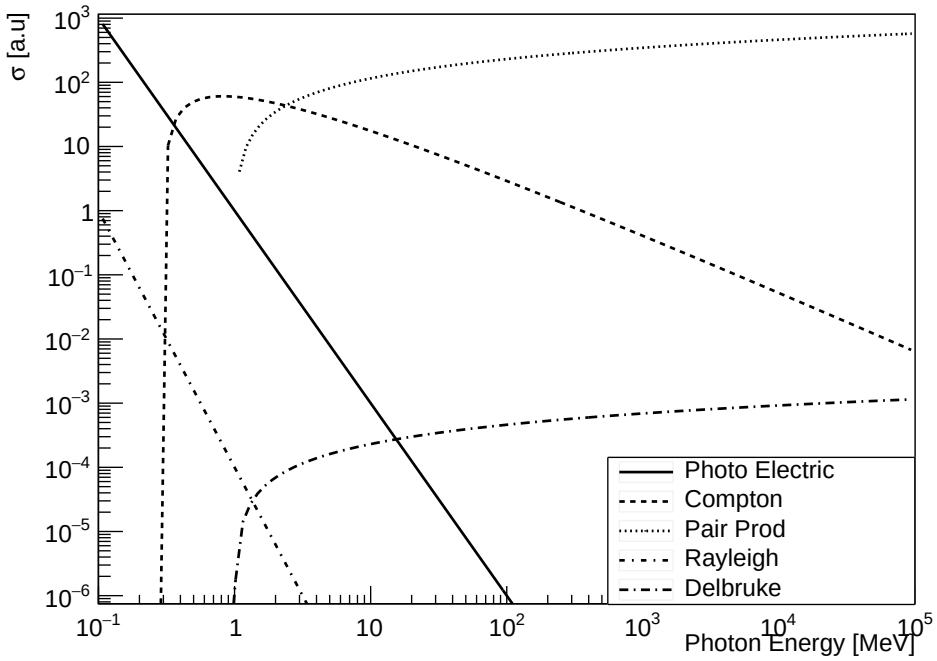

Figure 2.6: Differntial cross sections for various photon interaction plotted as a function of energy

2.5 Klein Nishina formula

Differential cross section $\frac{d\sigma}{d\Omega}$ measures the probability that a photon gets scattered into an angle θ

$$\frac{d\sigma}{d\Omega} = \frac{3}{16\pi}\sigma_T(\frac{\epsilon_f}{\epsilon_i})^2\left(\frac{\epsilon_i}{\epsilon_f} + \frac{\epsilon_f}{\epsilon_i} - \sin^2\theta\right)$$

where ϵ_i and ϵ_f are incident and scattered photon energies, σ_T is classical Thomas scattering cross section.

Figure 2.7 displays the simulation of the Klein Nishina cross section. The detailed route for the same can be found in appendix [6]. It is seen that with increasing photon energy (decreasing wavelength) the differential cross section decreases as well s the angle distributions asymmetrical, favoring forward scattering angles.

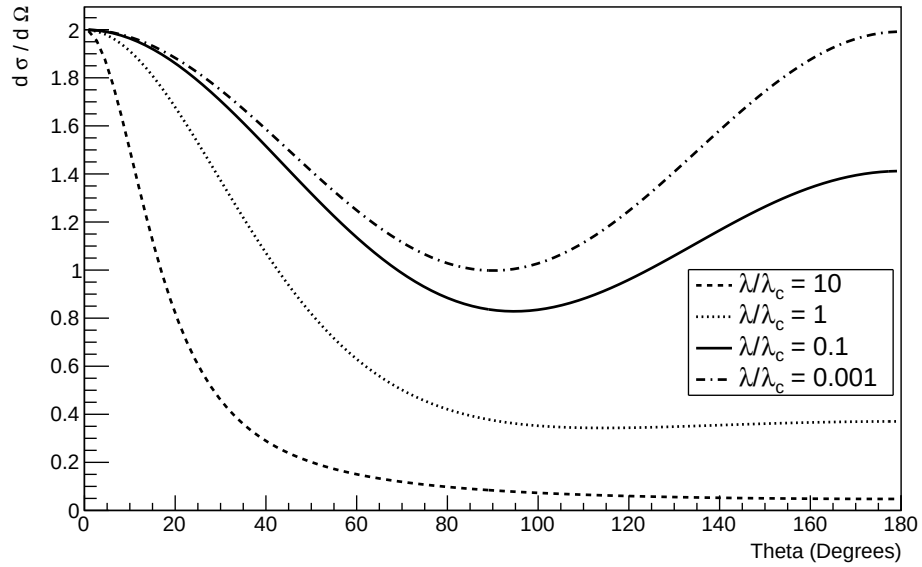

Figure 2.7: Variation of Klein Nishina cross sections with photon incident energy, λ_C is the compton wavelength. At high incident energy, forward scattering is favored.

Integrating over all the solid angle gives us the total cross section

$$\begin{aligned}\sigma &= \int \frac{d\sigma}{d\Omega} \sin\theta d\theta \\ &= \frac{3}{4}\sigma_T \left[\frac{1+x}{x^3}\left(\frac{2x(1+x)}{1+2x} - ln(1+2x) \right) + \frac{1}{2x} ln(1+2x) - \frac{1+3x}{(1+2x)^2} \right]\end{aligned}$$

where $x \equiv \frac{h\nu_i}{m_e c^2}$

The high energy and the low energy limits provide the cross sections for the Compton and Thomson scattering respectively.

$\sigma(x) \approx \sigma_T(1-2x)$ for $x << 1$ (Thomson)

$\sigma(x) \approx \frac{3}{8}\sigma_T \frac{1}{x}(ln(2x) + \frac{1}{2})$ for $x >> 1$ (Compton)

Chapter 3

Basic detector and pulse processing

The various components that convert the signals from the detector to produce the final gamma spectrum are summarised below

1. PreAmplifier: Three types: voltage sensitive, charge sensitive and current sensitive. It does not amplifies. The major function is matching impedance between detector(high impedance) and the rest of electronics(low impedance) for efficient coupling. This helps to maintain the signal-to-noise ratio. It only amplifies very small signals. Needs to be placed close to detector for the weak signals. The amplification factor is from few mV to tens of mV.

2. Semiconductors detectors require charge-sensitive pre amplifiers contrary to the voltage sensitive detectors for scintillators/gas detectors. This is because charge collection capacity (imaginary capacitance) of the semiconductor detectors varies with temperature and bias.

3. Amplifier/Shaper: amplies by a factor of 1000 from mV to V. Reshapes the exponential decay shaped pulses into gaussian. Advantage of Gaussian is less error and 95%confidence within 2 σ.

4. Shaper: identifies differential pulses and aids in removing the pile-up effects. It consists of a differentiator and an integrator. A choice of suitable time constant RC for the experiment ensure that the riser part of one pulse does not ride on the tail of the preceding pulse. Shaper improves S/N and restores signal height.

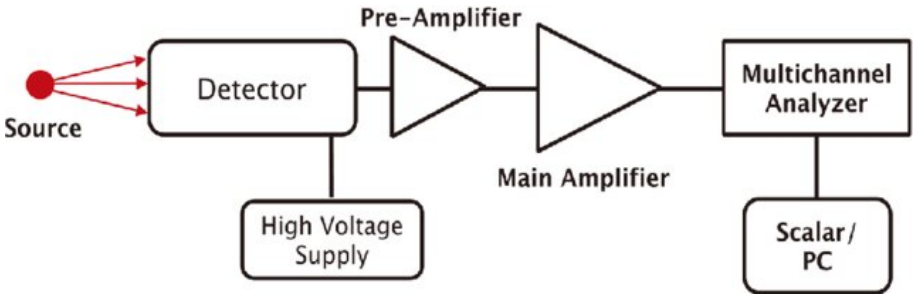

Figure 3.1: Block Diagram showing the pulse processing from the detector to the computer

5. SCA: Single Channel Analyser converts the analog pulse heights into digital channel numbers. A multi channel analyses is a collection of many SCA's, memory flip flops and ADC(analog to digital) converter.

6. MCA: It has faster data collection but slower data processing compared to SCA. The overall resolution consists of the detector resolution (fixed) and electronic resolution. The latter can be increased by having more channels in the MCA.

Chapter 4

Semiconductor detector and HPGe Clover

Various types of detectors are available depending on the use case and experiment of interest such as gas detectors, solid-state state detectors and liquid detectors.

4.1 Why Semiconductors?

Depending on the interaction probability the γ rays can travel over long distances attenuated, this limits the use of gaseous detectors as the active volume dimensions to capture the γ rays is around 1m for 1 MeV γ. For a scintillator this reduces to 100 cm while for a semiconductor crystal the required volume is only 100 mm.

The semiconductor detectors have an edge in the number of charge carriers generated for a fixed γ energy. For a incident 1 MeV γ, around 2×10^6 compared to 2×10^4 in the gaseous detectors. This difference arises from the small band gap in semiconductors. The high number of charge carriers (n) so produced reduces the FWHM($\frac{1}{\sqrt{(n)}}$) and improves the energy resolution of the detector.

The charge carries in semiconductors are electron and holes as compared to electrons and ions in gaseous detectors. The electron and holes are produced in same magnitude and acts as carrier of same magnitude. This reduces the charge collection time enabling processing of high event rate.

4.2 HPGe detectors

The high Z = 32 of the germanium over silicon enhances their gamma interaction probability as presented in the Chapter 2. Specifically we use, extrinsic semiconductors to enhance the electrical conductivity.

The width of the depletion (d) region formed at the p-n junction is obtained by solving the Poisson equation as

$$d = \sqrt{\frac{2\epsilon V}{N}}$$

here, V is the applied voltage bias, ϵ is the permittivity of vacuum and N is the impurity concentration.

The depletion width (d) is significantly increases with reduction in the impurity N as shown in above equation. This justifies the use of highly pure germanium detector in gamma spectroscopy having an impurity concentration of 10^{10} atoms / cm^3.

For our project all the crystals were n-type and operated in reverse bias to ensure no charge carriers without an external source.

4.3 HPGe clover

The HPGe detectors have lower detector efficiency due to smaller germanium crystal. The γ collection efficiency can be enhanced by producing larger sized crystal or using smaller crystals as a composite detector. The later is preferred as its technically feasible as well offers a couple of other advantages such as reduced doppler brodenning, polarity measurements [4] [5] [6].

A clover shown in Figure 4.1 is a specific type of composite detector comprising of four Ge crystals arranged in four-leaf Clover shape. The four crystals are fitted in a single housing and mounted on a common cryostat. Each crystal is around 5cm (diameter) and 7 cm (length).

The individual detector signals needs be calibrated for accounting the drifts in energy response before they can be merged into a single signal. This energy calibration has been performed and discussed in next chapter. The signal can be

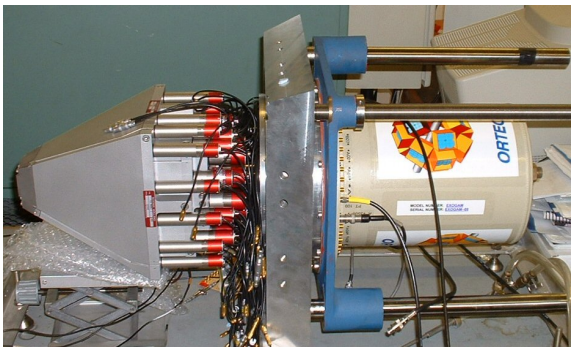

(a) a

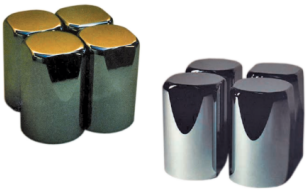

(b) b

Figure 4.1: (a) EXOGAM clover detector [8]. (b) Germanium crystal arrangement inside a clover

merged in two modes,

1. Sum = Crystal 1 + Crystal 2 + Crystal 3 + Crystal 4

2. Addback: In this mode the signals from individual detectors are summed within a time window on an event by event basis. This enables the reconstruction of photopeaks from individual crystal compton scattering. The gain in efficiency as compared to the sum mode is defined by an addback factor that is significantly high at high energies. The addback factor is the ratio of the counts under a photopeak in the addback to the counts under the same photopeak in sum mode.

Further increase in photopeak efficiency can be achieved by suppressing compton escape peaks using an active BGO shield which veto the Germanium signal.

Chapter 5

Data processing and analysis

5.1 Peak Identification

Standard sources of ^{133}Ba and ^{152}Eu are used for energy calibration owing to them emitting large number of γ rays across a wide energy range of 80 keV to 1408 keV, thus making the fit reliable. Prior to fitting, it is important to identify the peak energies with corresponding centroids. For this we identified the 1408 keV γ as the significant highest energy peak and then obtained the other peak energies using unitary method. The result of this exercise for all the four crystals is presented in Figure 5.3.

5.2 Energy Calibration

Energy calibration involves obtaining a relation between the ADC channel number and the corresponding γ energy. The advantage of shifting from channel numbers to γ energy is to make the experimental measurements setup independent and making the comparison and evaluation of the results from different facilities feasible.

The Radware GF3 program [9] was used to extract the peak centroids, areas and FWHM with corresponding uncertainties. The peak centroids were plotted against the corresponding γ energies(E_{ref}) taken from the `Eu152.sou` file in Radware directory. The experimental data points were fit using ROOT program [10]. The

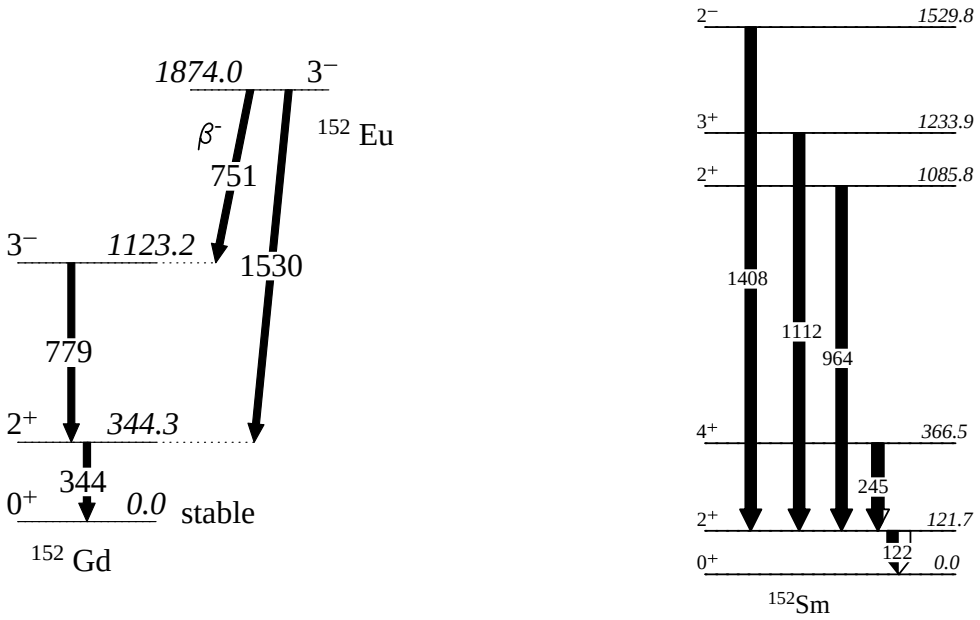

(a) a (b) b

Figure 5.1: ^{152}Eu decay scheme showing the transitions used for analysis

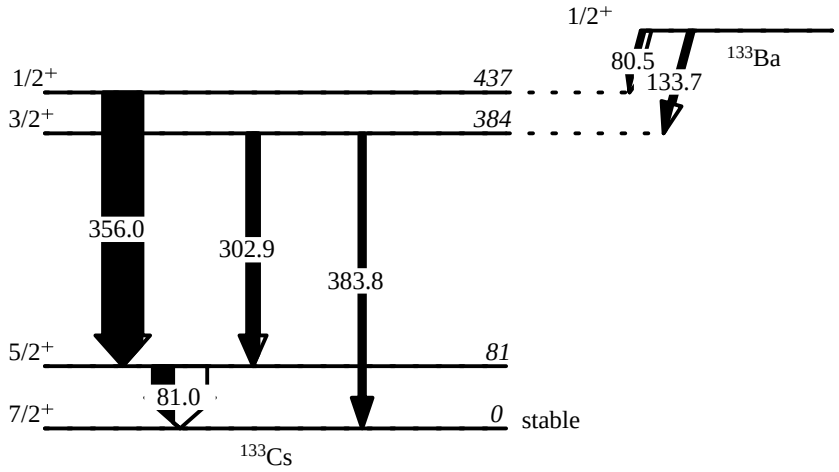

Figure 5.2: ^{133}Ba isotope level scene from GLS program showing the transitions used for analysis

crystal number 21 in clover 4 was not working hence it was not calibrated.

The experimental data points with a linear

$$E = p0 + p1 \cdot x \tag{5.1}$$

and a quadratic polynomial

$$E = p0 + p1 \cdot x + p2 \cdot x^2. \tag{5.2}$$

Here x is the channel number of the ADC and $p0$, $p1$ and $p2$ coefficients of the polynomials.

The reliability of fit is evaluated by the deviations(residual) plot with the residual evaluated as

$$Residual(\%) = 100 \times \frac{E_{ref} - Efit}{E_{ref}}$$

For the present analysis, it has been found that, both the linear and quadratic fitting have no significant difference on the residuals as also seen in residual plots of

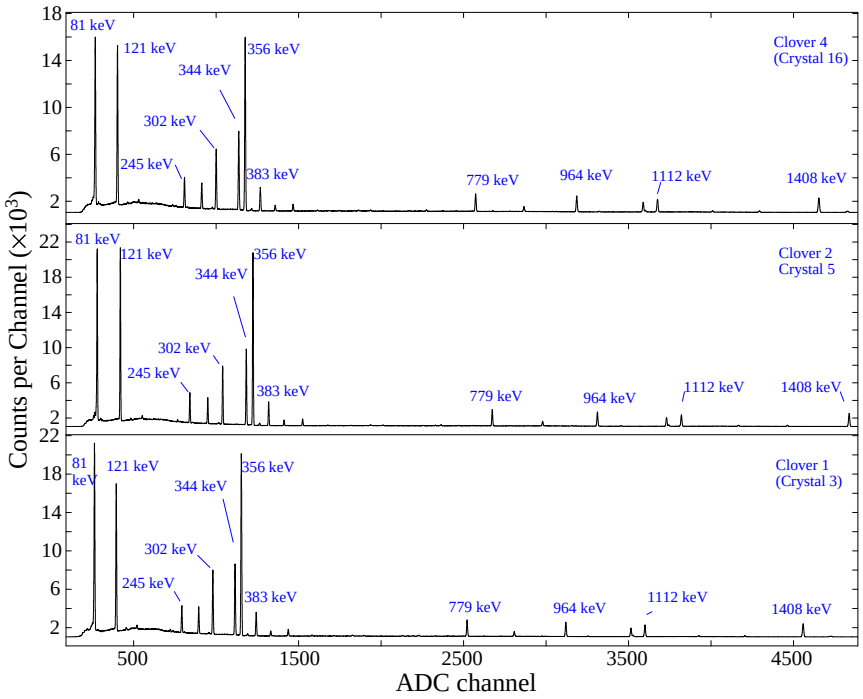

Figure 5.3: Uncalibrated spectra the drifts in the different clover crystals

Figures Figures 5.5 and 5.4 present the energy calibration along with the residuals and the fitting parameters.

5.3 Energy Resolution

Energy resolution of germanium is combined effect of three effects, inherent statistical spread in number of charge carriers, variations in the charge collection efficiency and electronic noise. The full width at half maximum (W) is given as

$$W^2 = (2.35)^2 F \epsilon E_\gamma \tag{5.3}$$

Here, F is the Fano factor, ϵ is the energy required to produce one electron hole pair and E_γ is the photon energy. Figure 5.7 shows the trend of the peak widths (obtained using *gf3*) with corresponding γ energy. Overall, the FWHM increases with the energy. A linear fit was made to experimental measurements for each of four crystals.

5.4 Addback

Following the calibration of individual crystals the signals were merged by sum and addback process. The addback factor was calculated by ratio of counts under peak in the addback vs sum specra. The `PK` command in GF3 was used getting reasonably accurate peak areas. The errors in the addback factor were propaged as

$$\Delta\text{add-back} = (\text{add-back}) \times \sqrt{\left(\frac{\Delta E}{E}\right)^2 + \left(\frac{\Delta\text{Area}}{\text{Area}}\right)^2} \tag{5.4}$$

The comparison in the counts in the addbback and sum spectra is shown in Figure 5.9. Figure 5.10 presents the variation of addback factor with energy. There is a clear increase above 200 keV owing to increased compton cross sections followed by reduction photopeak counts. The sharp rise slows as high energies due to reduction in Compton scattering and possibility of peak escaping the crystal.

Table 5.1: Energy Calibration Parameters for the 6 clovers

Crystal	p0	p1	p2
c1	-0.640	0.302	-1.585E-07
c2	-0.656	0.307	-1.550E-07
c3	-0.543	0.310	-1.095E-07
c4	-0.818	0.319	-2.422E-07
c5	1.774	3.430	2.742E-06
c6	-0.142	0.295	-2.256E-08
c7	-0.345	0.296	-4.713E-08
c8	8.560	0.294	2.876E-06
c9	-0.242	0.322	3.472E-09
c10	-0.206	0.332	4.678E-08
c11	-0.203	0.309	-5.595E-08
c12	-0.185	0.324	1.950E-08
c13	-0.242	0.322	3.472E-09
c14	-0.206	0.332	4.678E-08
c15	-0.203	0.309	-5.595E-08
c16	-0.185	0.324	1.950E-08
c17	-0.388	0.302	-2.146E-08
c18	-0.759	0.302	-1.315E-07
c19	2.496	0.299	3.038E-07
c20	-0.296	0.306	-8.572E-08
c22	3.299	2.663	6.274E-06
c23	-0.727	0.381	-1.703E-07
c24	-0.809	0.385	-2.229E-07

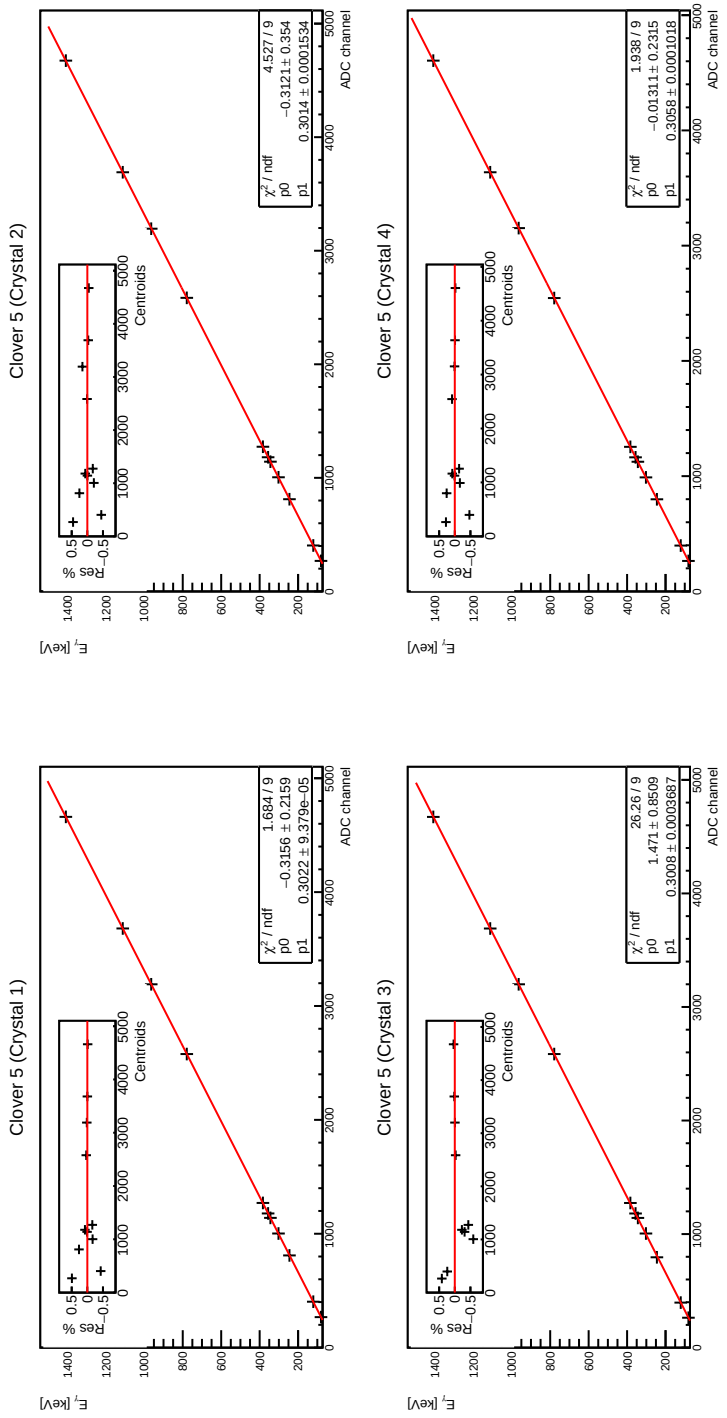

Figure 5.4: Energy calibration of Clover 5 using a linear fit function. Inset shows the deviation to the fit.

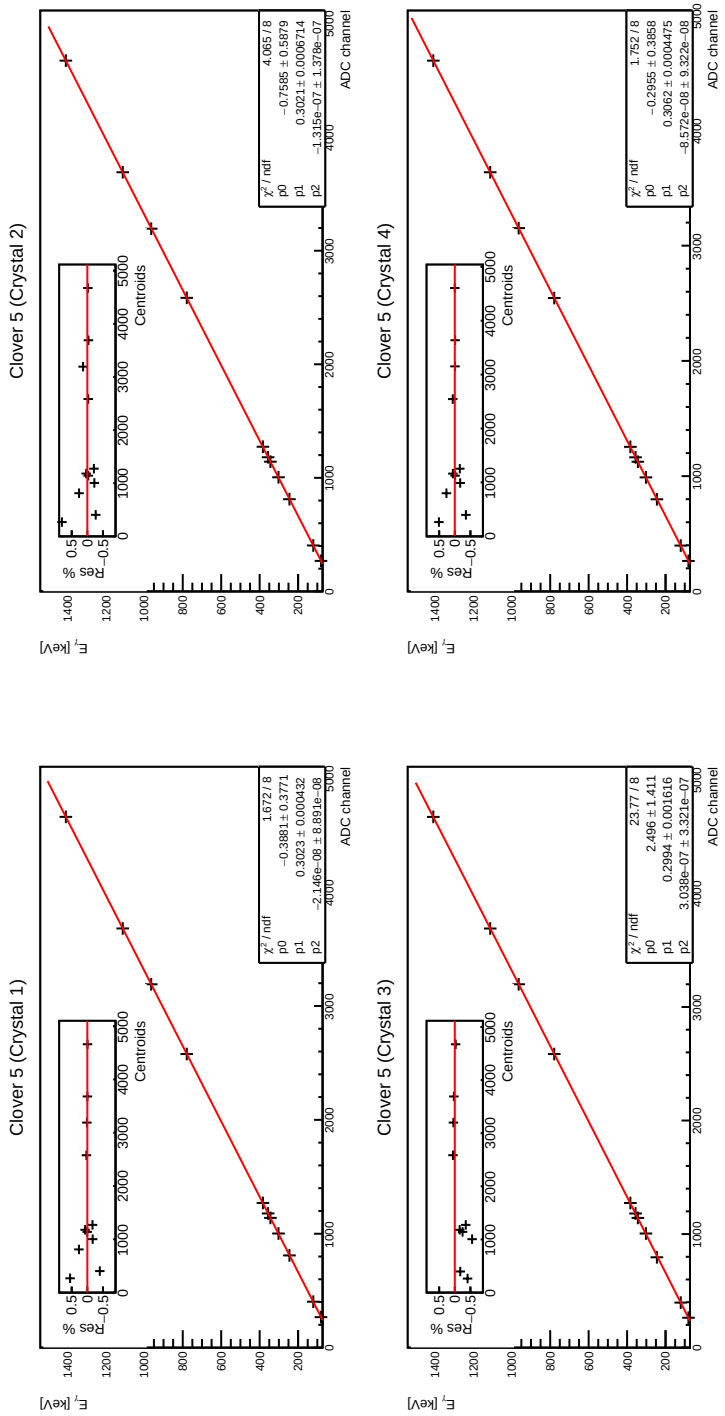

Figure 5.5: Energy calibration of Clover 5 using a quadratic fit function. Inset shows the deviation to the fit.

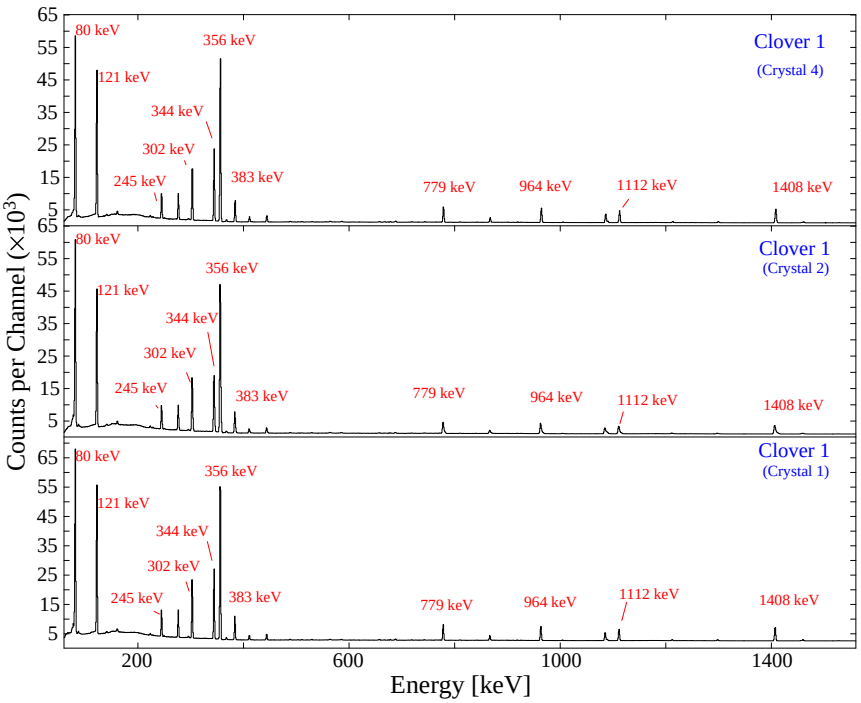

Figure 5.6: Calibrated spectra for Clover 1

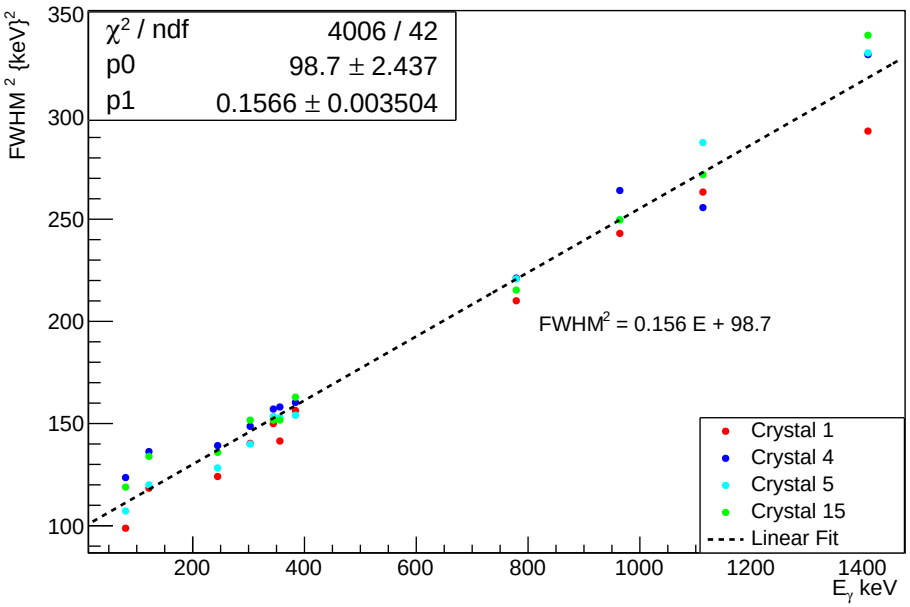

Figure 5.7: Variation of FWHM squared with energy fitted with linear function.

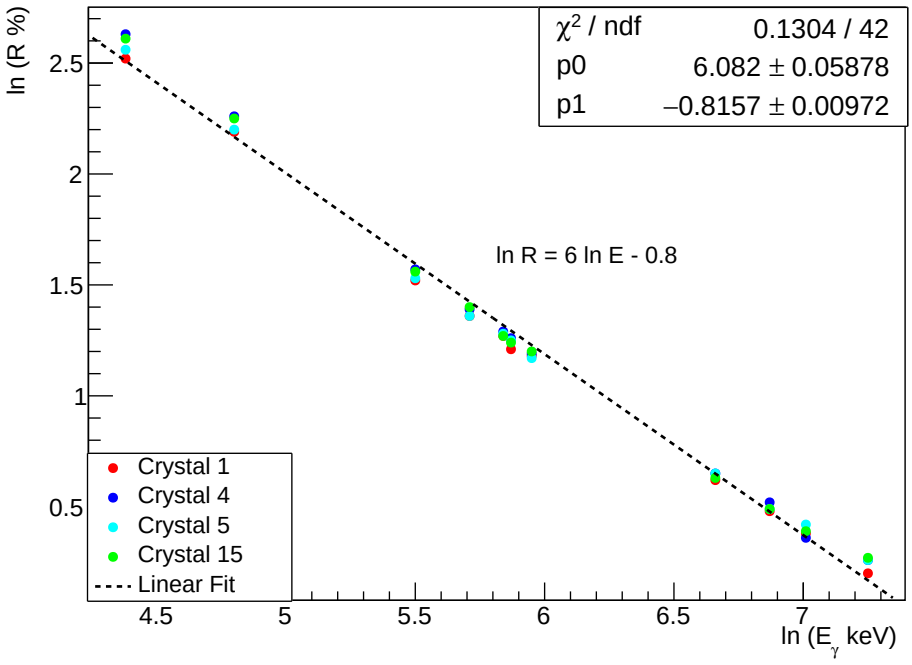

Figure 5.8: Resolution variation with energy fitted with a linear function.

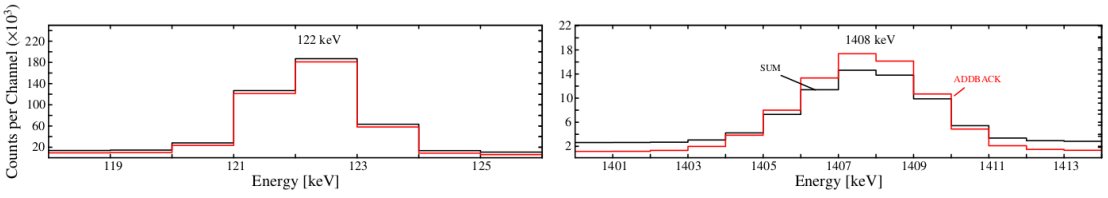

Figure 5.9: Comparison of the counts in the sum and addback spectra at low energy(122 keV) and high energy(1408 keV).

Table 5.2: Addback Factors and energies

Energy	Addback factor	Error
80.9	0.98	0.01
121.8	1.00	0.01
244.7	1.04	0.01
302.9	1.09	0.01
344.3	1.11	0.01
356.0	1.12	0.01
383.9	1.14	0.01
778.9	1.28	0.01
964.1	1.31	0.01
1112.8	1.33	0.01
1408.0	1.35	0.01

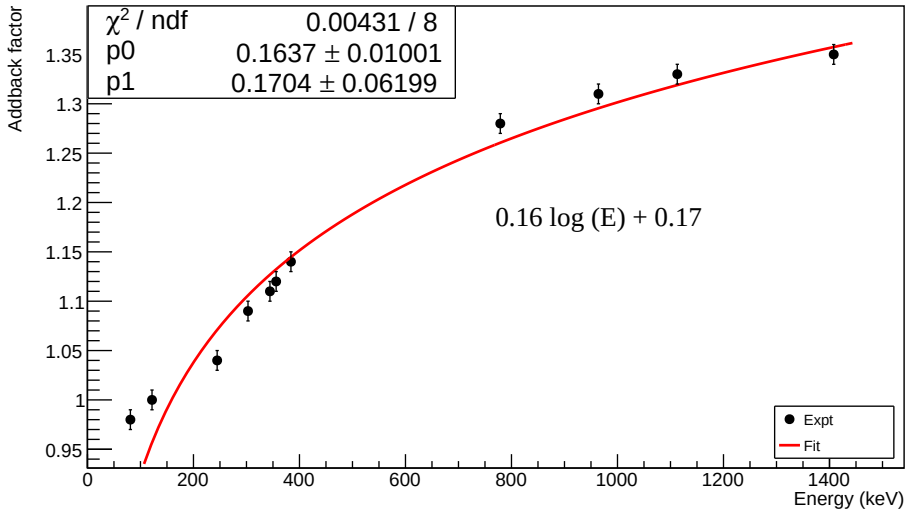

Figure 5.10: Energy dependence of the addback factor

Chapter 6

Conclusion and Summary

Clover detectors with their excellent resolution and enhanced photopeak efficiency, high peak to total ratio through addback and compton impression are very crucial in building complex level schemes and deducing nuclear structure of exotic nuclides. Their compact nature make them ideal for applications such as soil characterisation, radiation monitoring etc. Large array of Gamma detectors such as Gammasphere comprising of different types of segmented HPGe detectors holds the future of Gamma-ray spectroscopy measurement technique across the globe.

The individual clover crystals have been calibrated using a linear and quadratic function. Based on the deviation plots the present analysis founds that a higher order polynomial does not significantly improves the goodness fit and a linear function itself may be used for a decent analysis. The calibrated energy spectra shows that the relative spectra are free from drifts and is very important prior to fitting.

The comparison of counts in the peak at 121 keV and 1408 keV reveals that addback factor may not be significant at low energies and may even slightly reduce the counts. However above 100 keV as the compton scattering probablity increases, the counts and photopeak efficiency in addback increases sharply. The rate of increase gradually slows at high energy ($> 1MeV$) due to reduction in compton and more escaping γ rays. The addback factor table and plot also support these conclusions.

The addback factor may slightly decrease the resolution due to summing however the enhancement in the photopeak is quite high as compared to individual or composite detector.

The fundamental characteristics of a HPGe detectors have studied, followed by merging the signals from individual detectors and understanding the importance of the addback mode in enhancing the detector photopeak efficiency. In future we

would like to perform the efficiency calibration of the detector as well as validate the experimental results via Monte Carlo simulations.

Appendix

Simulation of Klein Nishina cross section

```
#include <iostream>
#include <cmath>
#include <TCanvas.h>
#include <TF1.h>
#include <TStyle.h>

double klein_nishina_function(double *x, double *par) {
    double theta = x[0];
    double E = 1/(1 + par[0]*(1 - cos(theta)));
    return E * E * (E + 1/E - sin(theta)*sin(theta));
}

void klein_nishina() {
    TCanvas *canvas = new TCanvas("", "", 800, 600);

    gStyle->SetLineColor(kBlack);

    TF1 *f4 = new TF1("f3", klein_nishina_function, 0, TMath::Pi(), 1);
    f4->SetParameter(0, 10);
    f4->SetLineStyle(2); // Set dashed line style
    f4->Draw();

    TF1 *f3 = new TF1("f2", klein_nishina_function, 0, TMath::Pi(), 1);
    f3->SetParameter(0, 1);
    f3->SetLineStyle(3); // Set dotted line style
    f3->Draw("same");


    TF1 *f1 = new TF1("f1", klein_nishina_function, 0, TMath::Pi(), 1);
    f1->SetParameter(0, 0.001);
    f1->SetLineStyle(5); // Set dash-dotted line style
    f1->Draw("same");

    TF1 *f2 = new TF1("f4", klein_nishina_function, 0, TMath::Pi(), 1);
```

```
    f2->SetParameter(0, 0.1);
    f2->SetLineStyle(1); // Set dash-dotted-dotted line style
    f2->Draw("same");

    f1->GetXaxis()->SetTitle("Theta"); // Set x-axis label
    f1->GetYaxis()->SetTitle("Value"); // Set y-axis label
    canvas->SetGrid(); // Enable grid

    TLegend *legend = new TLegend(0.7, 0.7, 0.9, 0.9);
    legend->AddEntry(f4, "#lambda/#lambda_{c} = 10", "l");
    legend->AddEntry(f3, "#lambda/#lambda_{c} = 1", "l");
    legend->AddEntry(f2, "#lambda/#lambda_{c} = 0.1", "l");
    legend->AddEntry(f1, "#lambda/#lambda_{c} = 0.001", "l");
    legend->Draw();

    canvas->Update();
}

}
```

RADWARE Screen dump

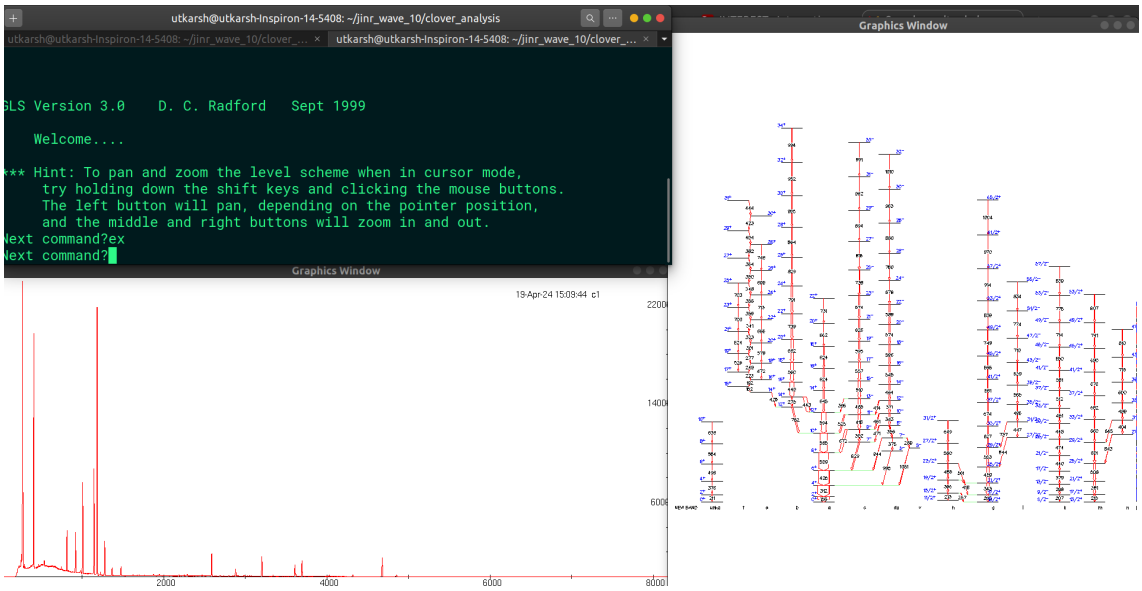

Figure 6.1: Radware screen dump showing the GF3 and the GLS program

Peak Fitting

The GF3 offers peak fitting through

1. `AF`: The simplest way to define a fit in gf3 is to use the command AF. This command will iteratively search the spectrum for peaks, perform a least-squares fit, search again for more peaks (this time on the difference between the least-squares fit), re-fit, etc. This continues until no more viable peaks are found.

2. `NF` : We just choose the fit limits and then indicate the peak locations until you have entered as many peaks as you wish (up to the maximum of 15). Then, type X or hit the third mouse button and the fit will proceed. When the fit has been completed such information as the limits, number of peaks and iterations, and chi-square will be listed on the terminal. Provided that the fit converged, these data will also be written to the print file.

In general, AF or NF is used to define new fits to regions of spectra, while FT is used to redo fits after they have been modified (with, for example, the commands AP, DP, FX, FR, MA etc.). The AF command is a relatively new feature; it provides a very easy and fast way of setting up new fits. NF is an alternative, less automated, way to define fits. Before using either of these commands, you should first display on the screen the portion of the spectrum which you wish to fit. The command FT has three slightly different functions, depending on whether it is followed by an integer that is: (a) greater than zero, (b) nonexistent (or zero), or (c) -1.

Getting Peak Counts

The `PK` commands offers a relatively simple way to obtain the peak area with the background subtraction. This is ideal for efficiency calibration and calculation of the addback factors. The command PK attempts to automatically determine the background below the peak, and the optimum peak integration limits. You will prompted to click with the cursor/mouse to select peaks that you wish to integrate; for isolated, reasonably strong peaks, clicking within one half-width is usually sufficient. For each peak integrated, the background and integration limits used are

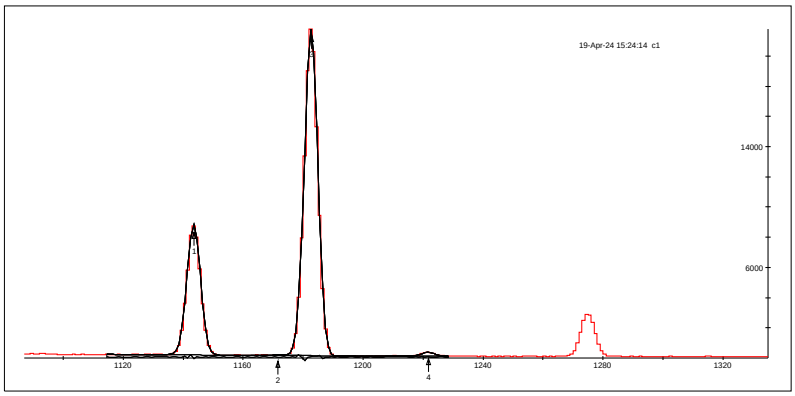

Figure 6.2: GF3 auto fit

```
Background: A = 111(7),   B = -0.02(17),   C = 0.0073(17)
     Shape: R = 9(15),   Beta = 0.9(5),   Step = 0.35(4)
  position      width       height        area          centroid      energy
1 1143.08(9)    5.11(3)     8636(53)      47525(249)    1143.001(11)  571.500(6)
2 1171.0(7)     2.8(12)     27(13)        84(39)        1170.9(7)     585.5(3)
3 1182.21(9)    5.11(3)     21655(86)     119175(436)   1182.126(7)   591.063(4)
4 1221.18(13)   4.62(17)    263(12)       1311(61)      1221.10(9)    610.55(5)
```

Figure 6.3: Fit Parameters

drawn on the spectrum display.

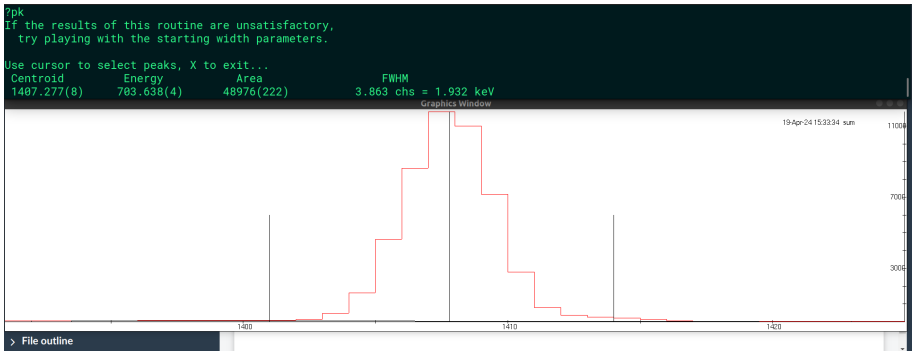

Figure 6.4: PK command for getting the peak area

Bibliography

[1] Milstein, A.I. *et al* . Present status of Delbrück scattering. Physics reports, **243** (4), 183-214 (1994).

[2] N. Kemmer, "Über die Lichtstreuung an elektrischen Feldern nach der Theorie des Positrons," Helv. Phys. Acta **10**, 112-122 (1937)

[3] Papatzacos, P. *et al* (1975). Delbrück scattering. Physics Reports , **21** (2), 81-118.

[4] P.K Joshi *et al* Study of the characteristics of a clover detector, Nuclear Instruments and Methods in Physics Research Section A: Accelerators, Spectrometers, Detectors and Associated Equipment , **399**, 51-56 (1997)

[5] G. Duchêne *et al* The Clover: a new generation of composite Ge detectors, Nuclear Instruments and Methods in Physics Research A **432**, 90-110 (1999)

[6] Beck, F. A., *et al* The clover detector (1992)

[7] Hubbell, J.H. and Seltzer, S.M. (2004), Tables of X-Ray Mass Attenuation Coefficients and Mass Energy-Absorption Coefficients (version 1.4)

[8] Nuclear Physics Group, University of Liverpool https://ns.ph.liv.ac.uk/ns-instrum-exogam-det.html

[9] Radware, David Radford's RadWare nuclear physics data analysis software. https://github.com/radforddc/rw05/tree/main

[10] Rene Brun and Fons Rademakers, ROOT - An Object Oriented Data Analysis Framework, Proceedings AIHENP'96 Workshop, Lausanne, Sep. 1996, Nucl. Inst. & Meth. in Phys. Res. A 389 (1997) 81-86.